Synergistic Charge Dynamics and Light Harvesting in TiO_2/MgO Composites for Efficiency Enhancement in CdS Quantum Dot-Sensitized Solar Cells

N.F. Ajward*, J.V.P. Fernando and V.P.S. Perera
Department of Physics, The Open University of Sri Lanka, Nawala, Nugegoda
nf2010.ajward@gmail.com, jvfer@ou.ac.lk & vpper@ou.ac.lk

ABSTRACT

Quantum dot-sensitized solar cells (QDSSCs) represent a promising advancement in renewable energy technologies, with recent improvements achieving power conversion efficiencies close to 6%. Structurally similar to dye-sensitized solar cells (DSSCs), QDSSCs employ quantum dots (QDs) as sensitizers that absorb photons and inject excited electrons into the conduction band of a wide-bandgap semiconductor electrode, while the redox electrolyte removes the generated holes and completes the circuit through regeneration at the counter electrode. Quantum dots composed of materials such as CdS, CdSe, PbS, and InP are increasingly studied for use in QDSSCs, offering the advantage of tunable optical band gaps through particle size manipulation. This adaptability enhances QDSSCs' design potential, enabling the integration of third-generation solar cell configurations, including multiple exciton generation (MEG), to further improve energy conversion efficiency.

Despite these advancements, QDSSC performance is currently limited by issues such as reduced photovoltage and recombination losses at the TiO_2-QD-electrolyte interface. This study investigates the effect of MgO incorporation into TiO_2 photoanodes on the photovoltaic performance of CdS QDSSCs, with particular attention to the fill factor (FF) and overall cell efficiency. MgO is expected to act as an interfacial passivation layer suppressing combination and improving charge-selective transport. In addition, MgO may enhance light scattering within the photoanode, thereby improving light harvesting and short-circuit current density.

In this study, MgO powder was incorporated in specific mass ratios with TiO_2, followed by the application of CdS quantum dots (QDs) on the TiO_2/MgO composite layer using the SILAR method. Results indicated a significant improvement in the fill factor (FF) at an optimal MgO-to-TiO_2 ratio, attributed to synergistic effects of MgO on interface stabilization, reduced recombination, and enhanced charge transport. The optimized MgO-modified TiO_2 films achieved a current density of 1.95 mA cm-2, voltage of 437 mV, and power of 0.121 mW (active area = 0.49 cm^2), reaching an efficiency of 0.311 % (18.7% higher than TiO_2/CdS QDSCs), with improved interfacial impedance, Incident Photon to Current Efficiency (IPCE), and FF of 0.374.

KEYWORDS: *QDSCs, MgO, TiO_2, CdS, SILAR, efficiency, Fill factor.*

1 INTRODUCTION

Quantum dot-sensitized solar cells (QDSCs) represent a promising class of third-generation photovoltaic technologies, offering cost-effective fabrication, tunable optical properties, and potential for enhanced energy conversion via mechanisms such as multiple exciton generation. Structurally analogous to dye-sensitized solar cells (DSSCs), QDSCs replace organic dyes with semiconductor quantum dots (QDs), which absorb incident photons and inject excited electrons into the conduction band of a wide-bandgap semiconductor, typically TiO_2. The redox electrolyte simultaneously extracts holes and regenerates the QDs, completing the electrochemical circuit (Sambur & Parkinson, 2010).

The use of QDs such as CdS, CdSe, PbS, and InP has gained traction due to their size-dependent bandgap tunability and high extinction coefficients, enabling broader spectral absorption than conventional dyes (Sargent, 2005; Beard et al., 2007). Among them, CdS quantum dots are widely used owing to their favorable band alignment with TiO_2 and straightforward synthesis via methods such Successive Ionic Layer Adsorption and Reaction (SILAR). However, QDSCs still suffer from performance limitations caused by rapid charge recombination at the TiO_2–QD–electrolyte interfaces and low open-circuit voltages (Chen et al., 2012; Gao et al., 2017).

https://doi.org/10.54389/VYTG1962

To address these challenges, recent studies have explored interfacial engineering strategies, including the introduction of wide-bandgap metal oxide layers such as MgO. MgO coatings have demonstrated an ability to suppress interfacial recombination, improve charge selectivity, and enhance light scattering within the photoanode structure, thereby boosting both the short-circuit current and fill factor (Wang et al., 2014; Chang et al., 2016). Furthermore, insulating nature of MgO can act as an electron-blocking layer, mitigating electron back-transfer and increasing the carrier lifetime in the system (Liu & Kamat, 1993).

Although MgO has previously been explored as a passivation or buffer layer in semiconductor-based solar cells, systematic optimization of the MgO–TiO_2 composition for CdS-based QDSSCs has received limited attention. In this work, MgO was incorporated into TiO_2 photoanodes at different mass ratios to identify the optimum composition for enhanced photovoltaic performance. CdS quantum dots were deposited by the SILAR method, and the resulting photoanodes were evaluated through photovoltaic, electrochemical, structural, and optical characterization to correlate MgO content with charge transport, recombination behavior, and light-harvesting properties.

2 EXPERIMENTAL DETAILS

2.1 Preparation of TiO2/MgO Films Varying Mass Ratio

MgO powder was measured according to the quantities specified in Table 1. For each sample, concentrated HNO_3 acid was added dropwise to the MgO powder which was then ground in a mortar and pestle. TiO_2 powder 0.25 g was subsequently mixed with one drop of Triton X-100, and 0.05 g of PEG 1000. The resulting paste was spread onto pre-cleaned conducting tin oxide (CTO) glass plates (1.0 cm × 2.0 cm) using the doctor blade method. The cleaning process involved ultrasonic bath treatment with detergent and distilled water. Finally, the TiO_2 coated films were dried on a hot plate and sintered in a furnace at 450 °C for 45 minutes

Table 1. Mass of MgO for each sample

Sample	**1**	**2**	**3**	**4**	**5**	**6**	**7**	**8**	**9**
Mass of MgO(g)	0.0025	0.0050	0.0075	0.0100	0.0125	0.0150	0.0175	0.0200	0.0225
Percentage	1%	2%	3%	4%	5%	6%	7%	8%	9%

2.2 Deposition of CdS using SILAR method.

To prepare solutions containing precise concentrations of Cd^{2+} and S^{2-} ions, 10.065 g of $CdCl_2$ and 3.902 g of Na_2S were weighed with an electronic balance (±0.001 g accuracy). These compounds were then dissolved in 100 ml of distilled water. To optimize the solubility of the relevant species and enhance the electrochemical behavior within the cell, the pH of the $CdCl_2$ solution was adjusted to 4.5. This was achieved by carefully adding 0.01 M NaOH or 0.01 M HCl solutions dropwise while closely monitoring the pH.

The SILAR method was employed to deposit CdS films on the TiO_2/MgO photoanodes. Each dipping step into the $CdCl_2$ and Na_2S solutions lasted for one minute. After each dip, the photoanodes were rinsed with distilled water to remove any excess reagents, then air-dried. To ensure uniform film formation, the photoanodes were then dipped in the complementary precursor solution (anionic or cationic), followed by a washing and drying cycle. This entire sequence of steps was repeated ten times to make a multilayered CdS film. Finally, the coated photoanodes were heated on a hot plate at 80 °C for 30 minutes to enhance the film's stability and adhesion to the substrate.

2.3 Preparation of Electrolyte

2ml of electrolyte solution was prepared by combining 0.1301g of Na_2S, 0.1283g of S, and 0.0301g of KCl mixed in Methanol (1.4ml) and distilled water (0.6ml) as solvents. The mixture was stirred for three (3) hours using a magnetic stirrer to ensure complete dissolution of the components and prevent sulfur precipitation of. The stirring time might require adjustment if sulfur precipitation is observed.

2.4 Fabrication of the cell

Conducting side of Pt counter electrode was placed face-to-face with the CdS coated TiO_2 or TiO_2/MgO film and secured with two clamps. The space between the electrodes was then filled with the electrolyte solution, completing the QDSSC assembly.

2.5 Characterization

The fabricated QDSSCs were rigorously characterized using a VK-PA-100 PV Power Analyzer to obtain J–V curves, from which key photovoltaic parameters including photo-conversion efficiency (PCE), short-circuit current density (Jsc), open-circuit voltage (Voc), and fill factor (FF) were extracted. To ensure reproducibility, a minimum of five devices per batch were evaluated. Electrochemical Impedance Spectroscopy (EIS), conducted with an Auto lab Nova 2.1 frequency response analyzer, was employed to investigate charge transport and recombination mechanisms over a frequency range of 0.1 Hz to 1 MHz under simulated solar illumination. This provided critical insight into interfacial resistance and electron lifetime within the photoanode. The Incident Photon-to-Current Efficiency (IPCE) was assessed using a VK-IPCE-10 system to determine the wavelength-dependent photo response and light-harvesting efficiency of the devices.

In addition to electrochemical and photovoltaic analyses, comprehensive structural and morphological characterizations were performed. X-ray Diffraction (XRD) was used to examine the crystallinity and phase composition of the composite materials, At the same time Fourier Transform Infrared Spectroscopy (FTIR) provided information on chemical bonding and surface modifications. Scanning Electron Microscopy (SEM) was utilized to observe the surface morphology and distribution of MgO within the TiO_2/CdS matrix, confirming uniform dispersion and structural refinement. These combined techniques enabled a holistic understanding of the material properties and their influence on the overall performance of the QDSSCs.

3 RESULTS AND DISCUSSION.

3.1 I–V characteristics of CdS QDSSCs

Figure 1(a) presents the current-voltage (I-V) and 1(b) power-voltage (P-V) characteristics of TiO_2/MgO/CdS thin films containing varying MgO mass content, ranging from 1% to 9%.

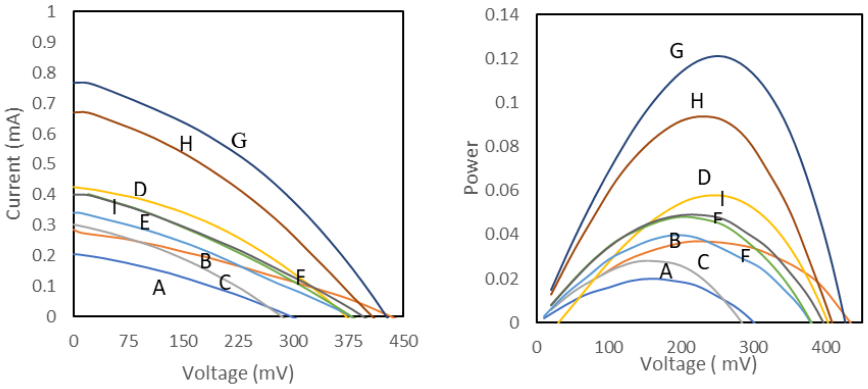

1(a) current-voltage (I-V) characteristics 1(b) power-voltage (P-V) characteristics

[A-MgO 1%, B-MgO 2%, C-MgO 3%, D-MgO 4%, E-MgO 5%, F-MgO 6%, G-MgO 7%, H-MgO 8% and I-MgO 9%,]

Figure 1(a) Current-voltage (I–V) plot for mass ratios ranging from 1% to 9%. (b) Power-voltage (P–V) plot for mass ratios from 1% to 9%.

Table 02: The photovoltaic data obtained for different mass ratio ranging from 1% to 9%

	1%	2%	3%	4%	5 %	6%	7%	8%	9%
V_{oc} (mV)	299.6	433.4	283.8	372	379.3	380.2	437	408.5	396.3
Jsc (mA $cm^{-2)}$	0.521	0.718	0.739	0.867	0.872	1.019	1.946	1.698	1.014

FF	0.323	0.307	0.346	0.369	0.307	0.316	0.374	0.349	0.316
η (%)	0.05	0.096	0.073	0.119	0.101	0.122	**0.311**	0.242	0.127
Power(mW)	0.02	0.037	0.028	0.058	0.04	0.048	**0.121**	0.094	0.049
V_{max} (mV)	160.1	239.9	170.1	210.0	190.1	200.0	260.2	229.9	229.9
I_{max} (mA)	0.123	0.155	0.166	0.278	0.208	0.239	0.466	0.410	0.215

The incorporation of MgO into TiO_2 photoanodes influenced the photovoltaic performance of the CdS QDSSCs, with the effect strongly dependent on MgO content. Among the investigated compositions, the 7 wt.% MgO sample exhibited the best performance, delivering a maximum efficiency of 0.311%, which is 18.7% higher than that of the unmodified TiO_2/CdS QDSC (0.262%). This improvement is attributed to an optimized balance between recombination suppression, charge transport, and light-harvesting enhancement at this composition.

The solar cell efficiency (η) is determined by the fundamental photovoltaic parameters and is given by

$$\eta = \frac{Voc\ X\ I\,sc\ X\ \ FF}{Pin\ X\ S}$$

Where P_{in} is the incident light power density and S= 0.49cm^2 is the illuminated area of the photoanode. The fill factor of the device was calculated based on the relation,

$$\text{FF} = \frac{I\max\ X\ \ Vmax}{I\,sc\ X\ Voc}$$

The MgO coating acts as a buffer layer, blocking back electron transfer and thereby improving the fill factor. Figure 1 and Table 2 show that the MgO-coated TiO_2-based QDSC exhibited a higher fill factor (0.374) than the unmodified TiO_2/CdS QDSC (0.265). Therefore, the fill factor of MgO-coated TiO_2 based QDSCs is approximately 41.13% higher than that of TiO_2/CdS QDSCs.

Figure 1 and Table 2 show that the highest power output (0.121 mW) was obtained with a 7% variation in MgO mass. The performance enhancement observed at 7 wt.% MgO can be attributed to the formation of an effective passivation layer that suppresses interfacial recombination between TiO_2 and the electrolyte. Excessive MgO content, however, may hinder electron transport due to the insulating nature of MgO.

3.2 Electrochemical Impedance Spectroscopy of CdS QDSSCs

The Nyquist plot in Figure 2 illustrates the impedance behavior of the TiO_2/MgO/CdS composite material. EIS measurements were performed over the frequency range of 100 kHz to 0.1 Hz with an AC amplitude of 10 mV (rms) superimposed on the open-circuit potential at room temperature (25 ± 1 °C). As the MgO concentration increases, the semicircular arcs in the plot become more prominent, reflecting increased interfacial resistance. Moderate resistance improves recombination suppression, whereas excessive resistance (≥8 wt.% MgO) hinders charge transport (Chen et al., 2018). In contrast, lower MgO concentrations correspond to smaller arc diameters, suggesting reduced resistive and capacitive behavior. These frequency-dependent changes reveal the influence of MgO on conductivity and interfacial charge transfer within the photoanode structure (Wang et al., 2011; Zhang et al., 2020).

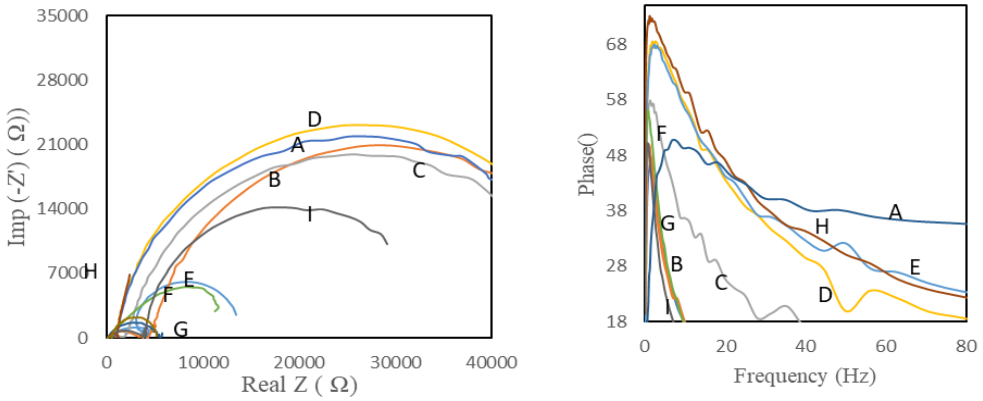

[A-MgO 1%, B-MgO 2%, C-MgO 3%, D-MgO 4%, E-MgO 5%, F-MgO 6%, G-MgO 7%, H-MgO 8% and I-MgO 9%,]

Figure 2(a) Impedance spectra characteristics of mass ratio MgO 1% to 9%

2(b) Phase-Frequency Plot for MgO Mass Ratios Ranging from 1% to 9%

According to the measured data, the TiO_2/CdS composite without MgO exhibited the lowest impedance, demonstrating superior charge transport properties. Upon MgO incorporation, a notable increase in impedance was observed, with the highest value recorded for the 8 wt.% MgO sample, indicative of excessive insulating behavior. The 7 wt.% MgO sample showed a decrease in impedance compared to 8 wt.%, highlighting its optimal composition for synergistic charge transport.

Figure 3 illustrates the series resistance (R_s) and polarization resistance (R_p) derived from circuit fitting, further supporting these observations. As shown in Table 3, the 7 wt.% MgO sample exhibits a very low Rs of 39 Ω, indicating enhanced bulk conductivity, and an Rp of 5.58 kΩ, reflecting a favorable balance between interfacial charge transfer and recombination suppression under the optimized MgO loading. (Roy-Mayhew et al., 2014; Villalva et al., 2009). A higher charge transfer resistance (Rp) indicates suppressed recombination at the semiconductor/electrolyte interface, thereby improving device performance. The optimized MgO composition exhibited the largest semicircle diameter, suggesting more efficient charge separation and reduced recombination losses.

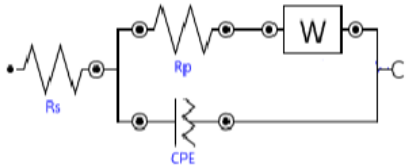

Figure 3: Equivalent Circuit Model for Nyquist Plot Fitting

Table 3. Parameters of equivalent circuit for different QDSC configuration EIS fitting parameters obtained from spectra measured at open-circuit under AM1.5G illumination (100 mW cm^{-2}). Device active area = 0.49 cm^2.

Parameters	1%	2%	3%	4%	5%	6%	7%	8%	9%
R_S (Ω)	2070	3130	1320	688	562	529	39	764	2710
R_P (kΩ)	120	51.6	48.6	49.6	48	41.7	5.58	134	32
CPE (n)	0.994	0.858	0.869	0.949	0.920	0.997	0.677	0.920	0.95
Phase (°) (Approx.)	49	50	68	69	49	48	30	48	44
Frequency at which phase peak observed.	10	9	5	4	10	10	100	10	10

Electrical parameters were reported with three significant figures, consistent with the measurement accuracy (~±3%). The TiO_2/MgO/CdS composite with 7% MgO exhibited notable deviation from ideal capacitive behavior, evidenced by its low CPE exponent of 0.677. A moderate phase angle (30°) near 10 Hz for the 7 wt.% MgO sample suggests a balanced system, effective charge transport combined with optimized interfacial capacitance and minimized recombination losses. Other MgO concentrations displaying either very high phase angles at low frequencies (indicating slow charge transfer or excessive capacitance) or very low phase angles at higher frequencies (reflecting resistive behavior or poor charge storage) are less optimal. This deviation likely results from increased interfacial roughness, composite inhomogeneities, or other structural factors introduced by MgO, impacting charge storage and transfer at the material interfaces.

3.3 Incident Photon-to-Current Efficiency (IPCE) of QDSSCS

Figure 4 illustrates the spectral response of the TiO_2/CdS/MgO composites at various MgO concentrations over the wavelength range of 500–600 nm. The plot indicates that the composite exhibits the highest response, particularly around 540 nm, with the 7% MgO concentration showing the highest

peak, suggesting enhanced light absorption or photon-to-electron conversion in this region. However, at higher MgO concentrations, particularly beyond 7%, the response diminishes, indicating that excessive MgO may disrupt charge separation and transfer efficiency, thereby reducing the composite's ability to effectively absorb light. Overall, the findings suggest that an optimal MgO concentration exists maximize the light absorption capabilities of the TiO_2/CdS/MgO composite, with the 7% MgO sample demonstrating a balance between absorption efficiency and material stability.

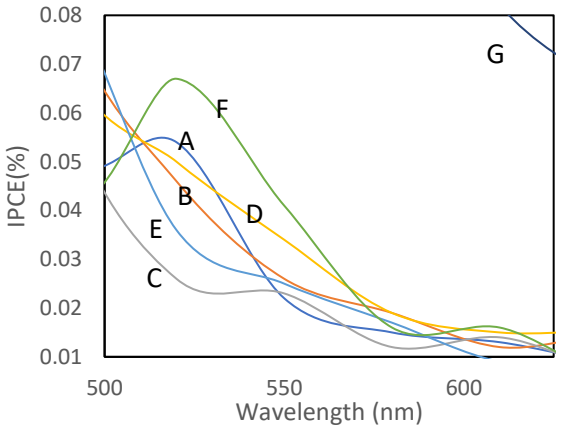

[A-MgO 2%, B-MgO 3%, C-MgO 4%, D-MgO 5%, E-MgO 6%, F-MgO 7%and G-MgO 8%]

Figure 4. Incident Photon-to-Current Efficiency (IPCE) of CdS Quantum Dot-Sensitized Solar Cells (QDSSCs) with various mass ratios of MgO, varying from 2% to 8%.

3.4 Scanning electron microscopy

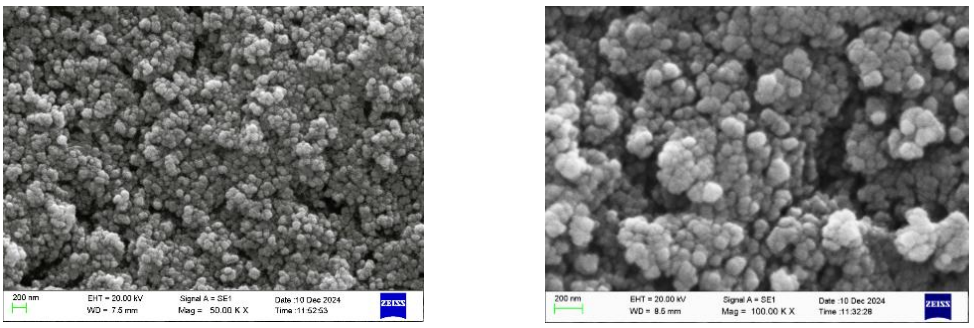

TiO_2 /CdS TiO_2 /CdS// MgO

Figure 5: SEM images of TiO_2/CdS and TiO_2/MgO/CdS 7% films used in quantum dot-sensitized solar cells (QDSSCs).

Figure 5 shows SEM images that clearly illustrate the morphological differences between TiO_2/CdS and TiO_2/MgO/CdS films used in quantum dot-sensitized solar cells (QDSSCs). In the TiO_2/CdS sample, the surface is composed of uniformly distributed, densely packed spherical nanoparticles with small diameters. This structure is advantageous for providing a large effective surface area, enhancing CdS quantum dot loading and light absorption (Wang et al., 2021). Surface roughness and nanoscale feature also facilitate strong interfacial contact for charge transfer.

Upon introducing 7 wt.% MgO, the TiO_2/MgO/CdS sample exhibited a noticeable increase in particle size and surface granularity. This morphological evolution suggests the formation of a conformal MgO layer, which may lead to nanoparticle coalescence or growth. MgO has been reported to reduce surface trap states and suppress electron–hole recombination, leading to improved charge separation and device performance (Zhang et al., 2020). Although the surface area may decrease slightly, the passivation and improved charge- transport pathways outweigh this limitation.

3.5 XRD and FTIR spectra of TiO_2/CdS and TiO_2/MgO/CdS

Figure 6 (a) presents the X-ray diffraction (XRD) patterns of TiO_2/CdS and TiO_2/MgO/CdS (7%) composite materials, revealing the crystalline characteristics of the synthesized samples. A prominent peak at $2\theta \approx 25.3°$ corresponds to the (101) plane of anatase TiO_2, in agreement with standard diffraction data (JCPDS No. 21-1272). Additional peaks in the 26°–38° range are assigned to CdS, which may include both

hexagonal and cubic phases (JCPDS No. 80-0019 and 10-0454, respectively; Nazeeruddin et al., 2003). The incorporation of 7% MgO leads to a noticeable increase in peak intensity and sharpness, suggesting improved crystallinity and reduced structural defects, potentially due MgO's role in stabilizing the lattice and promoting domain growth (Zhang et al., 2014). The absence of clear MgO peaks is likely due to its low concentration and possible amorphous nature, as similarly reported in literature (Chen et al., 2017).

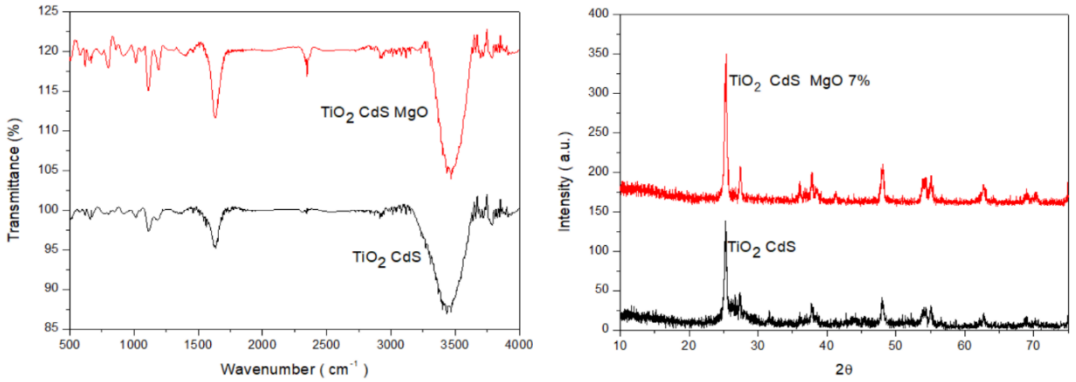

Figure 6: (a) X-ray Diffraction (XRD) patterns showing the crystalline structure of TiO_2, CdS, and the composite material TiO_2 CdS with 7% MgO.
(b) Fourier Transform Infrared (FTIR) spectra illustrating the vibrational modes of TiO_2 CdS and TiO_2 CdS with 7% MgO.

Figure 6(b) shows Fourier Transform Infrared (FTIR) spectra that illustrates vibrational changes upon MgO incorporation. A broad band around 3400 cm^{-1} in both spectra is attributed to O–H stretching vibrations from surface hydroxyl groups or adsorbed water (Nowak et al., 2010). In the MgO-modified sample, slight spectral shifts in this region may indicate the formation of Mg–OH bonds, thereby enhancing surface passivation. Ti–O–Ti and Cd–S stretching vibrations are observed below 800 cm^{-1}, although they may overlap in this range. The observed spectral changes in the TiO_2–CdS–MgO sample suggest alterations in bonding environments and successful MgO incorporation. Such modifications are expected to improve charge separation and reduce surface trap states, thereby enhancing the photovoltaic performance of quantum dot-sensitized solar cells (QDSCs) (Yu et al., 2015; Zhu et al., 2014).

4 CONCLUSION

The incorporation of MgO into TiO_2/CdS quantum dot-sensitized solar cells (QDSCs) enhances photovoltaic performance by modifying the photoanode's interfacial and optical properties. At an optimal loading of 7 wt.%, MgO achieves the highest efficiency (η = 0.311%), reflecting an 18.7% improvement over unmodified TiO_2/CdS systems. This enhancement is primarily attributed to MgO's passivation effect, which reduces interfacial charge recombination and promotes directional electron transport. X-ray diffraction (XRD) analysis confirms the preservation of crystalline phases in TiO_2 and CdS, while increased peak sharpness and intensity with MgO incorporation indicate enhanced crystallinity and structural order. Fourier transform infrared (FTIR) spectroscopy reveals shifts in O–H and metal–oxygen stretching bands, suggesting effective surface modification and reduced trap states.

Electrochemical impedance spectroscopy (EIS) supports these findings, showing reduced series resistance (Rs = 39 Ω), moderate polarization resistance (Rp = 5.58 kΩ), and a CPE exponent (n = 0.677) indicative of favorable interfacial heterogeneity. Scanning electron microscopy (SEM) reveals homogeneous distribution of MgO and improved surface morphology. Incident photon-to-current efficiency (IPCE) spectra demonstrate a significant enhancement around 540 nm for the 7 wt.% MgO sample, indicating improved light harvesting and photon-to-electron conversion. Furthermore, current–voltage (I–V) analysis confirms elevated short-circuit current density (Jsc = 1.946 mA/cm^2), open-circuit voltage (Voc = 0.43 V), and fill factor (FF = 0.374).

Collectively, these findings underscore the role of MgO as a multifunctional additive that optimizes structural, optical, and electronic properties, thereby enabling a robust and efficient QDSC architecture. Overall, the results demonstrate that optimizing MgO content in TiO_2 photoanodes is an effective strategy

for improving the structural, optical, and interfacial properties of CdS QDSSCs. Among the investigated compositions, 7 wt.% MgO provided the best overall performance, confirming the importance of composition control in interfacial engineering for enhanced quantum dot-sensitized solar cell efficiency.

REFERENCES

Sargent, E. H. (2005). Infrared photovoltaics made by solution processing. Nature Materials, 4, 377–378. https://doi.org/10.1038/nmat1375

Beard, M. C., Knutsen, K. P., Yu, P., Luther, J. M., Song, Q., Metzger, W. K., Ellingson, R. J., & Nozik, A. J. (2007). Multiple exciton generation in colloidal silicon nanocrystals. Nano Letters, 7(8), 2506–2512. https://doi.org/10.1021/nl071486l

Chen, H.-Y., Pan, C.-L., Lin, C.-L., & Lee, Y.-L. (2012). Effects of interface recombination on the performance of QDSSCs. The Journal of Physical Chemistry C, 116(12), 6974–6980. https://doi.org/10.1021/jp211337m

Gao, Y., Liu, C., Song, Y., Zhang, H., & Wang, W. (2017). Efficient quantum dot-sensitized solar cells using MgO interfacial layers. Solar Energy Materials and Solar Cells, 165, 145–153. https://doi.org/10.1016/j.solmat.2017.03.025

Wang, X., Wang, Y., Chen, H., & Ma, T. (2014). Surface passivation of MgO for efficient QDSSCs. Electrochimica Acta, 147, 186–192. https://doi.org/10.1016/j.electacta.2014.09.045

Chang, C.-H., Tseng, C.-H., & Su, C.-Y. (2016). Enhanced performance of CdS quantum dot-sensitized solar cells using TiO_2 photoelectrodes modified with a MgO buffer layer. ACS Applied Materials & Interfaces, 8(15), 9831–9838. https://doi.org/10.1021/acsami.5b12406

Liu, D., & Kamat, P. V. (1993). Photoelectrochemical behavior of thin ZnO films: Effects of sol–gel and electrodeposition methods. The Journal of Physical Chemistry, 97(46), 10769–10773. https://doi.org/10.1021/j100147a006

Chen, B., Yang, M., Priya, S., & Zhu, K. (2018). Origin of J–V hysteresis in perovskite solar cells. Journal of Physical Chemistry Letters, 9(22), 5561–5567. https://doi.org/10.1021/acs.jpclett.8b02171

Wang, P., Zakeeruddin, S. M., & Grätzel, M. (2011). Enhancement of charge transport in quantum dot-sensitized solar cells by interface engineering. Journal of Physical Chemistry C, 115(19), 9518–9525. https://doi.org/10.1021/jp202323s

Nowak, A. P., Rakoczy, R., & Kuśmierek, K. (2010). FTIR analysis of surface hydroxyl groups on metal oxide catalysts. Spectrochimica Acta Part A: Molecular and Biomolecular Spectroscopy, 76, 384–389. https://doi.org/10.1016/j.saa.2010.03.002

Roy-Mayhew, J. D., & Aksay, I. A. (2014). Graphene materials and their use in dye-sensitized solar cells. Chemical Reviews, 114(12), 6323–6348. https://doi.org/10.1021/cr400412a

Villalva, M. G., Gazoli, J. R., & Filho, E. R. (2009). Comprehensive Approach to Modeling and Simulation of Photovoltaic Arrays. IEEE Transactions on Power Electronics, 24(5), 1198–1208. https://doi.org/10.1109/TPEL.2009.201386

Zhang, J., Zhang, X., & Li, Y. (2020). MgO-modified photoanodes for enhanced quantum dot-sensitized solar cell performance. Solar Energy Materials and Solar Cells, 210, 110484. https://doi.org/10.1016/j.solmat.2020.110484

Nazeeruddin, M. K., Kay, A., Rodicio, I., Humphry-Baker, R., Müller, E., Liska, P., Vlachopoulos, N., & Grätzel, M. (2003). Conversion of light to electricity by cis-X_2bis(2,2'-bipyridyl-4,4'-dicarboxylate) ruthenium (II) charge-transfer sensitizers on nanocrystalline TiO_2 electrodes. Journal of Photochemistry and Photobiology A: Chemistry, 159(1), 131–138. https://doi.org/10.1016/S1010-6030(03)00164-4

Zhang, Y., Wang, L., Zhao, Y., & Li, H. (2014). Enhanced photocatalytic activity of MgO-doped TiO_2 nanocomposites. Materials Chemistry and Physics, 148, 371–377. https://doi.org/10.1016/j.matchemphys.2014.07.041

Zhu, R., Zhang, Q., Cao, G., & Wang, Y. (2014). Interface modification strategies for high-efficiency quantum dot-sensitized solar cells. Nano Energy, 4, 138–145. https://doi.org/10.1016/j.nanoen.2014.02.008

Chen, S., Li, D., Zhang, S., Liu, Y., & Yang, H. (2017). Structural and optical properties of MgO-modified nanocomposites. Journal of Alloys and Compounds, 703, 153–160. https://doi.org/10.1016/j.jallcom.2017.01.073